Investigation of poorly-damped conditions in VSC-HVDC systems

Georgios Stamatiou
Chalmers University of Technology
Dept. of Energy and Environment
Gothenburg, Sweden
georgios.stamatiou@chalmers.se

Massimo Bongiorno
Chalmers University of Technology
Dept. of Energy and Environment
Gothenburg, Sweden
massimo.bongiorno@chalmers.se

*Abstract***— The use of Voltage Source Converter based High Voltage DC (VSC-HVDC) links is regarded as a major step in facilitating long distance power transfer and integrating renewable energy sources, e.g. wind farms. Such systems may experience stability or poor damping related issues and a stability study is considered necessary. The differences in the operating concept between point-to-point connections that either transfer power between existing ac grids or connect a wind farm to the main ac grid, imply a difference in their dynamic behavior as well. This paper examines these two types of two-terminal VSC-HVDC systems, investigates the effect of the system parameters on the system's stability and focuses on poorly-damped conditions that may appear in the dc transmission.**

Keywords-HVDC; VSC; Stability; Damping; Wind.

I. INTRODUCTION

The increased energy demands in parallel with the fact that the energy resources and consequent power production are usually located far from the load centers, implies the transportation of bulk power over long distances. Furthermore, environmental concerns have put nations under pressure to create a more CO_2 free society. This has contributed to setting the wind energy as the fastest growing energy technology to date, with increasing potential for the future. The establishment of large wind-farm sites in areas with ample wind energy capacity, usually requires the wind turbines to be located in remote locations such as offshore, in great distance from the nearest main ac grid.

The introduction of VSC-HVDC in power systems has offered a breakthrough in terms of efficient power transportation between remote areas, as well in the controllability and stability of the power systems they are part of. In turn, the widespread use of power electronic devices can also give rise to unwanted interactions between the different controllers and other parts of the system. Potential resonances might appear that can degrade the dynamic performance of the system and increase the risk of instability. Such occurrences have been described e.g. as oscillations caused by HVDC terminals [1] or instabilities in dc power systems [2].

This work was supported by ABB Power Systems, the Nordic Council through the OffshoreDC program.

In conventional two-terminal HVDC connections between power systems, one station controls the level of the direct-voltage in the dc-transmission link while the other controls the amount of active power to be transferred. A different strategy is applied, when it comes to interconnecting wind farms. The station connected to the main ac grid still controls the dc-link voltage but the station at the wind-farm collection point operates as an ac slack-bus, by controlling its ac voltage in terms of magnitude, phase and frequency. This change in strategy causes a different dynamic behavior of the combined system.

This paper investigates the dynamics of VSC-HVDC systems, focusing on poorly-damped conditions that may appear. In particular, the paper focuses on poorly-damped conditions in the dc transmission. The main interest is to observe how the VSC control parameters and the passive components of the system, as well as the nominal operating points, contribute to the relocation of the closed-loop poles. Consequently, it will be possible to define the conditions under which the poles of the system become poorly-damped. The investigation is applied to typical two-terminal VSC-HVDC systems, following the conventional strategy of direct voltage and active power control and VSC-HVDC connections to wind farms. In both cases, the interconnected system are modelled and their interaction are shown by means of pole movement, where the effect of the system parameters in creating poorly-damped poles is highlighted.

II. SYSTEM DESCRIPTION

A two-terminal VSC-HVDC transmission, will vary in its functionality and control, according to the application it is designed for. Therefore, the cases where such a link is established to connect two existing ac grids or a wind farm to a mainland grid, must be examined independently.

A. VSC-HVDC connecting existing ac grids

A typical two-terminal VSC-HVDC transmission system connecting two ac grids is depicted in Fig. 1(a). The system is a symmetrical monopole connection, comprised of two VSC stations, as well as ac and dc side components. Each station is assumed to be connected to a strong ac grid at the Point of Common Coupling (PCC), via a phase reactor and a

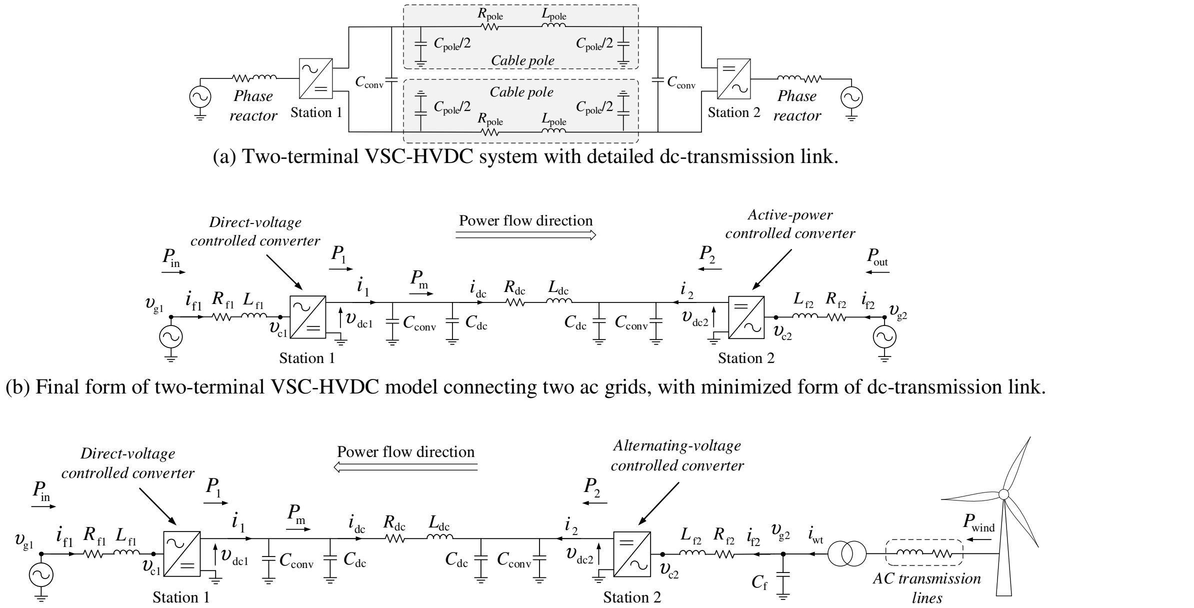

(a) Two-terminal VSC-HVDC system with detailed dc-transmission link.

(b) Final form of two-terminal VSC-HVDC model connecting two ac grids, with minimized form of dc-transmission link.

(c) Final form of two-terminal VSC-HVDC model connecting an aggregated wind farm to the mainland grid with minimized form of dc-transmission link.

Fig. 1. Two-terminal VSC-HVDC models.

step-up transformer. Considering that the ac grid is strong and the transformer has a low leakage inductance, they are both replaced by a voltage source to which the phase reactor is connected. The dc side of each station is connected to a capacitor bank C_{conv}. Each dc pole is modeled as a Π-model with resistance R_{pole}, inductance L_{pole} and capacitance C_{pole}, with values that are proportional to the length of the cable.

Assuming balanced operational conditions, the model in Fig. 1(a) can be equated to the asymmetrical monopole model in Fig. 1(b), which will be used further on in this paper. The cable Π-model has now the values $R_{dc}=2\cdot R_{pole}$, $L_{dc}=2\cdot L_{pole}$, and $C_{dc}=C_{pole}/4$. In the typical configuration of a two-terminal VSC-HVDC link, if power is transmitted from Station 1 to Station 2, then Station 1 is a direct-voltage controlled station and Station 2 is active-power controlled. In case of power flow reversal, the previous control duties are swapped between the stations. These controllers generate reference signals for the inner Current Controller (CC).

The dynamics of the active-power transfer in Station 2 are naturally independent from the dynamics of the direct-voltage control and the dc circuit. This happens because, for linear operation of the station, the flow of P_{out} (which is to be controlled) and the associated P_2 is related only to properties of the active-power controller, the CC and the physics of the associated ac-grid structure adjacent to the VSC of Station 2. None of these consider properties of the dc side to finally apply the desired P_{out}^* at the Point of Common Coupling (PCC). Therefore, the active-power controlled VSC acts as an ideal power source, transferring power P_2 between its dc and ac side, with P_2 seen as an externally provided input by the rest of the system.

B. VSC-HVDC connecting wind turbines

The connection of a wind farm to the offshore mainland via a two-terminal VSC-HVDC connection is presented in Fig. 1(c). Even though fairly similar in structure and control to the one in Fig. 1(b), the main difference is identified on the connection of Station 2 to the wind farm. This Station is operating in alternating-voltage control mode, trying to establish a desired alternating voltage v_{g2} across a filter capacitor C_f, where the wind farm is connected via transmission lines and a transformer.

A control scheme for this type of control mode can be found in [3], where a feedforward term from the measured wind farm current i_{wf} ensures that the closed loop dynamics of v_{g2} are not affected by the dynamics of i_{wf}. Consequently, Station 2 provides a slack-bus for the wind farm to be connected to. Any power from the wind farms will then simply propagate through the converter and injected to its dc side as P_2. For similar reasons as in the case of the two-terminal VSC-HVDC connection between two ac grids, the dynamics of the ac side of Station 2 are isolated from those of the dc-side of the connection. Therefore, P_2 can again be seen as an externally provided input by the rest of the system. It should be noted here that the direction of the power for a connection to a wind farm is from Station 2 to Station 1, with the latter being in direct-voltage control mode. This opposite to the case with the transfer of power between two established ac grids and will have an impact on the dc-system dynamics.

III. SYSTEM DYNAMICS

As observed in the previous section, the dynamics associated with the power-controlled station and the alternating-voltage controlled station are decoupled from those of the rest of the system, which is however identical for both cases of the VSC-HVDC transmission. The only difference is the direction of power flow with respect to the position of the direct-voltage controlled station in the system. Therefore, a common model for the dc-side dynamics can be developed for the two types of VSC-HVDC systems and the analysis will be based on the scheme of Fig. 1(b).

A. DC-transmission link dynamics

For this analysis, the two VSC stations can be represented as controllable current sources with Station 1 injecting current $i_1=P_1/v_{dc1}$ and Station 2 injecting $i_2=P_2/v_{dc2}$, as depicted in Fig. 1(b). The capacitors C_{conv} and C_{dc} on the side of each converter have a lumped value of C_{tot}. Considering Station 1, the direct-voltage dynamics are

$$C_{\text{tot}}\frac{dv_{\text{dc1}}}{dt}=\frac{P_1}{v_{\text{dc1}}}-i_{\text{dc}}\Rightarrow C_{\text{tot}}\frac{d\Delta v_{\text{dc1}}}{dt}=\frac{1}{v_{\text{dc1,0}}}\Delta P_1-\frac{P_{1,0}}{v^2_{\text{dc1,0}}}\Delta v_{\text{dc1}}-\Delta i_{\text{dc}}\Rightarrow$$
$$\frac{d\Delta v_{\text{dc1}}}{dt}=\frac{1}{C_{\text{tot}}v_{\text{dc1,0}}}\Delta P_1-\frac{1}{C_{\text{tot}}R_{10}}\Delta v_{\text{dc1}}-\frac{1}{C_{\text{tot}}}\Delta i_{\text{dc}} \quad (1)$$

where the term $v^2_{\text{dc1,0}}/P_{1,0}$ has been replaced with R_{10}. The subscript "0" denotes the steady-state value of an electrical entity, around which the latter is linearized, and is consistently used in the rest of the analysis in the thesis. The dynamics of the v_{dc2} on the dc side of Station 2 are

$$C_{\text{tot}}\frac{dv_{\text{dc2}}}{dt}=i_{\text{dc}}+\frac{P_2}{v_{\text{dc2}}}\Rightarrow C_{\text{tot}}\frac{d\Delta v_{\text{dc1}}}{dt}=\frac{1}{v_{\text{dc2,0}}}\Delta P_2-\frac{P_{2,0}}{v^2_{\text{dc2,0}}}\Delta v_{\text{dc2}}+\Delta i_{\text{dc}}\Rightarrow$$
$$\frac{d\Delta v_{\text{dc2}}}{dt}=\frac{1}{C_{\text{tot}}v_{\text{dc2,0}}}\Delta P_2-\frac{1}{C_{\text{tot}}R_{20}}\Delta v_{\text{dc2}}+\frac{1}{C_{\text{tot}}}\Delta i_{\text{dc}} \quad (2)$$

Similarly, the term $v^2_{\text{dc2,0}}/P_{2,0}$ has been replaced with R_{20}. The dynamics of the current i_{dc} are

$$L_{\text{dc}}\frac{di_{\text{dc}}}{dt}=R_{\text{dc}}i_{\text{dc}}-v_{\text{dc2}}+v_{\text{dc1}}\Rightarrow\frac{d\Delta i_{\text{dc}}}{dt}=\frac{R_{\text{dc}}}{L_{\text{dc}}}\Delta i_{\text{dc}}-\frac{1}{L_{\text{dc}}}\Delta v_{\text{dc2}}+\frac{1}{L_{\text{dc}}}\Delta v_{\text{dc1}} \quad (3)$$

The state-space model of the considered dc-transmission system is created by considering (1)-(3). The states of the system are $x_1=\Delta v_{\text{dc1}}$, $x_2=\Delta i_{\text{dc}}$ and $x_3=\Delta v_{\text{dc2}}$. The inputs are $u_1=\Delta P_1$ and $u_2=\Delta P_2$. For $W=v^2_{\text{dc1}}$, the output of the system is $y=\Delta W=2v_{\text{dc1,0}}\Delta v_{\text{dc1}}$. The resulting state-space model is

$$\mathbf{A}_{\text{dc-link}}=\begin{bmatrix}-\frac{1}{C_{\text{tot}}R_{10}} & -\frac{1}{C_{\text{tot}}} & 0\\ \frac{1}{L_{\text{dc}}} & \frac{R_{\text{dc}}}{L_{\text{dc}}} & -\frac{1}{L_{\text{dc}}}\\ 0 & \frac{1}{C_{\text{tot}}} & -\frac{1}{C_{\text{tot}}R_{20}}\end{bmatrix},\ \mathbf{B}_{\text{dc-link}}=\begin{bmatrix}\frac{1}{C_{\text{tot}}v_{\text{dc1,0}}} & 0\\ 0 & 0\\ 0 & \frac{1}{C_{\text{tot}}v_{\text{dc2,0}}}\end{bmatrix} \quad (4)$$
$$\mathbf{C}_{\text{dc-link}}=\begin{bmatrix}2v_{\text{dc1,0}} & 0 & 0\end{bmatrix},\ \mathbf{D}_{\text{dc-link}}=0$$

The output, as a function of the two inputs, is then

$$\Delta W=\left[\boldsymbol{C}_{\text{dc-link}}\left(s\mathbf{I}-\mathbf{A}_{\text{dc-link}}\right)^{-1}\mathbf{B}_{\text{dc-link}}+\mathbf{D}_{\text{dc-link}}\right]\cdot\begin{bmatrix}\Delta P_1\\ \Delta P_2\end{bmatrix}\Rightarrow$$
$$\Delta W=\begin{bmatrix}H_1(s) & H_2(s)\end{bmatrix}\cdot\begin{bmatrix}\Delta P_1\\ \Delta P_2\end{bmatrix}\Rightarrow\Delta W=H_1(s)\Delta P_1+H_2(s)\Delta P_2 \quad (5)$$

B. AC-side dynamics

In this section, the ac-side dynamics of Station 1 and their interaction with the dc-transmission link is established. Assuming a lossless converter and power-invariant space-vector scaling [4] or p.u. quantities, the conservation of power on the dc- and ac-side of the converter implies the following relation in the rotating *dq*-frame that is synchronized with the PCC voltage v_{g1}

$$P_1=v^d_{\text{c1}}i^d_{\text{f1}}+v^q_{\text{c1}}i^q_{\text{f1}}\Rightarrow\Delta P_1=v^d_{\text{c1,0}}\Delta i^d_{\text{f1}}+i^d_{\text{f1,0}}\Delta v^d_{\text{c1}}+v^q_{\text{c1,0}}\Delta i^q_{\text{f1}}+i^q_{\text{f1,0}}\Delta v^q_{\text{c1}} \quad (6)$$

As mentioned earlier, the ac grid and transformer are jointly represented by a voltage source with a fixed frequency ω_{g1} and magnitude $v^d_{\text{g1}}+jv^q_{\text{g1}}$ on the converter *dq*-frame. Once the PLL has estimated the correct angle of its *dq*-frame, any power flow changes will not affect the measured angle and the effect of the PLL on the system disappears. Consequently, $v^q_{\text{g1}}=0$ and v^d_{g1} is constant over time. The ac-side dynamics are then

$$\begin{matrix}v^d_{\text{c1}}=v^d_{\text{g1}}-\left(R_{\text{f1}}+sL_{\text{f1}}\right)i^d_{\text{f1}}+\omega_{g1}L_{\text{f1}}i^q_{\text{f1}}\\ v^q_{\text{c1}}=-\left(R_{\text{f1}}+sL_{\text{f1}}\right)i^q_{\text{f1}}-\omega_{g1}L_{\text{f1}}i^d_{\text{f1}}\end{matrix}\Rightarrow\begin{matrix}\Delta v^d_{\text{c1}}=-\left(R_{\text{f1}}+sL_{\text{f1}}\right)\Delta i^d_{\text{f1}}+\omega_{g1}L_{\text{f1}}\Delta i^q_{\text{f1}}\\ \Delta v^q_{\text{c1}}=-\left(R_{\text{f1}}+sL_{\text{f1}}\right)\Delta i^q_{\text{f1}}-\omega_{g1}L_{\text{f1}}\Delta i^d_{\text{f1}}\end{matrix} \quad (7)$$

The steady-state values $v^d_{\text{c1,0}}$ and $v^q_{\text{c1,0}}$ can be derived as

$$\begin{matrix}v^d_{\text{c1,0}}=v^d_{\text{g1,0}}-R_{\text{f1}}i^d_{\text{f1,0}}+\omega_{g1}L_{\text{f1}}i^q_{\text{f1,0}}\\ v^q_{\text{c1,0}}=-R_{\text{f1}}i^q_{\text{f1,0}}-\omega_{g1}L_{\text{f1}}i^d_{\text{f1,0}}\end{matrix} \quad (8)$$

Inserting (7) and (8) into (6), provides the following expression for ΔP_1

$$\Delta P_1=\left[-i^d_{\text{f1,0}}\left(2R_{\text{f1}}+sL_{\text{f1}}\right)+v^d_{\text{g1,0}}\right]\Delta i^d_{\text{f1}}+\left[-i^q_{\text{f1,0}}\left(2R_{\text{f1}}+sL_{\text{f1}}\right)\right]\Delta i^q_{\text{f1}}\Rightarrow$$
$$\Delta P_1=-i^d_{\text{f1,0}}L_{\text{f1}}\left(s+b^d_1\right)\Delta i^d_{\text{f1}}-i^q_{\text{f1,0}}L_{\text{f1}}\left(s+b^q_1\right)\Delta i^q_{\text{f1}} \quad (9)$$

where

$$b^d_1=2\frac{R_{\text{f1}}}{L_{\text{f1}}}-\frac{v^d_{\text{g1,0}}}{L_{\text{f1}}i^d_{\text{f1,0}}},\ b^q_1=2\frac{R_{\text{f1}}}{L_{\text{f1}}} \quad (10)$$

For a CC designed as in [5], with closed-loop dynamics of a low-pass filter with bandwidth a_{cc}, the relation between *dq* current references and filter currents becomes

$$\Delta i^d_{\text{f1}}=\frac{a_{\text{cc}}}{s+a_{\text{cc}}}\Delta i^{d\,*}_{\text{f1}},\ \Delta i^q_{\text{f1}}=\frac{a_{\text{cc}}}{s+a_{\text{cc}}}\Delta i^{q\,*}_{\text{f1}} \quad (11)$$

It is assumed that $i^q_{\text{f1}}{}^*$ is constant and therefore $\Delta i^q_{\text{f1}}{}^*=0$. Thus, inserting (11) into (9) provides

$$\Delta P_1=-a_{\text{cc}}i^d_{\text{f1,0}}L_{\text{f1}}\frac{s+b^d_1}{s+a_{\text{cc}}}\Delta i^{d\,*}_{\text{f1}} \quad (12)$$

The direct-voltage controller of the station is designed as

$$P^*_{\text{in}}=K_{\text{p}}\left(W^*-W\right)+P_{\text{f}} \quad (13)$$

controlling the square of the voltage W, rather than v_{dc1}, as suggested in [5]. K_{p} is a proportional gain equal to $a_{\text{d}}C_{\text{conv}}/2$, where a_{d} is the desired bandwidth of the closed-loop direct-voltage control and P_{f} is the filtered feedforward power

$$P_{\text{f}}=H(s)P_{\text{m}} \quad (14)$$

with $H(s)=a_{\text{f}}/(s+a_{\text{f}})$ being a low pass filter of bandwidth a_{f}. The actual power P_{in} will gradually follow its reference P_{in}^*. This power is different from P_1 because of the reactor resistance R_{f1} and the associated power loss. The steady-state value of the feedforward term P_{f} is equal to P_1. Therefore, the controller needs an integrator with a very low gain K_{i} to compensate for the small steady-state deviation between P_{in} and P_1. For very low values of K_{i}, the integrator has negligible effect on the overall dynamics and can here be assumed to be zero [5]. The reference power P_{in}^* is

$$P^*_{\text{in}}=v^d_{\text{g1}}i^{d\,*}_{\text{f1}} \quad (15)$$

which when inserted to (13) gives

$$P^*_{\text{in}}=v^d_{\text{g1}}i^{d\,*}_{\text{f1}}=K_{\text{p}}\left(W^*-W\right)+P_{\text{f}}\Rightarrow v^d_{\text{g1,0}}\Delta i^{d\,*}_{\text{f1}}=K_{\text{p}}\left(\Delta W^*-\Delta W\right)+\Delta P_{\text{f}}\Rightarrow$$
$$\Delta i^{d\,*}_{\text{f1}}=\frac{K_{\text{p}}\left(\Delta W^*-\Delta W\right)+\Delta P_{\text{f}}}{v^d_{\text{g1,0}}} \quad (16)$$

Relations (12) and (16) provide the final expression for the injected power to the dc-transmission link

$$\Delta P_1=K(s)\left[K_{\text{p}}\left(\Delta W^*-\Delta W\right)+\Delta P_{\text{f}}\right] \quad (17)$$

with

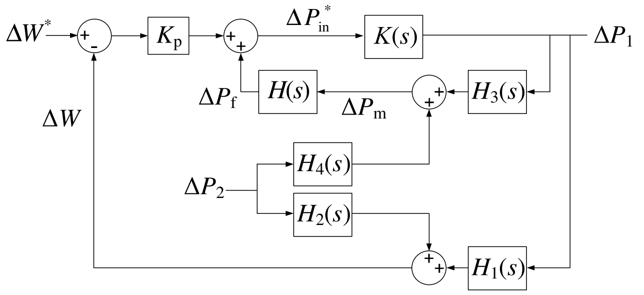

Fig. 2 Block diagram representation of the two-terminal VSC-HVDC control process.

$$K(s) = -\frac{a_{cc} i_{f1,0}^{d} L_{f1}}{v_{g1,0}^{d}} \frac{s + b_1^d}{s + a_{cc}} \tag{18}$$

Given (14), the filtered power ΔP_f can be expressed as

$$\Delta P_f = H(s) \Delta P_m \tag{19}$$

Based on the arrangement of Fig. 1(b), the dc-side powers are related in the following way

$$\left.\begin{array}{l} \frac{C_{conv}}{2}\frac{dW}{dt} = P_1 - P_m \\ \frac{C_{dc}}{2}\frac{dW}{dt} = P_m - v_{dc1} i_{dc} \end{array}\right\} \Rightarrow \frac{P_1 - P_m}{C_{conv}} = \frac{P_m - v_{dc1} i_{dc}}{C_{dc}} \Rightarrow P_m = \frac{C_{dc}}{C_{tot}} P_1 + \frac{C_{conv}}{C_{tot}} v_{dc1} i_{dc} \Rightarrow$$

$$\Delta P_m = \frac{C_{dc}}{C_{tot}} \Delta P_1 + \frac{C_{conv} v_{dc1,0}}{C_{tot}} \Delta i_{dc} + \frac{C_{conv} P_{1,0}}{C_{tot} v_{dc1,0}} \Delta v_{dc1} \tag{20}$$

Considering the same dc-grid system as in the previous section with the same inputs ΔP_1 and ΔP_2 but new output ΔP_m as in (20), the new state-space representation becomes

$$\mathbf{A}_{dc} = \begin{bmatrix} -\frac{1}{C_{tot} R_{10}} & -\frac{1}{C_{tot}} & 0 \\ \frac{1}{L_{dc}} & \frac{R_{dc}}{L_{dc}} & -\frac{1}{L_{dc}} \\ 0 & \frac{1}{C_{tot}} & -\frac{1}{C_{tot} R_{20}} \end{bmatrix}, \mathbf{B}_{dc} = \begin{bmatrix} \frac{1}{C_{tot} v_{dc1,0}} & 0 \\ 0 & 0 \\ 0 & \frac{1}{C_{tot} v_{dc2,0}} \end{bmatrix} \tag{21}$$

$$\mathbf{C}_{dc} = \begin{bmatrix} \frac{C_{conv} P_{1,0}}{C_{tot} v_{dc1,0}} & \frac{C_{conv} v_{dc1,0}}{C_{tot}} & 0 \end{bmatrix}, \mathbf{D}_{dc} = \begin{bmatrix} \frac{C_{dc}}{C_{tot}} & 0 \end{bmatrix}$$

The output ΔP_m, as a function of the two inputs, is then

$$\Delta P_m = \left[\boldsymbol{C}_{dc} \left(s\mathbf{I} - \mathbf{A}_{dc} \right)^{-1} \mathbf{B}_{dc} + \mathbf{D}_{dc} \right] \cdot \begin{bmatrix} \Delta P_1 \\ \Delta P_2 \end{bmatrix} \Rightarrow$$

$$\Delta P_m = \begin{bmatrix} H_3(s) & H_4(s) \end{bmatrix} \cdot \begin{bmatrix} \Delta P_1 \\ \Delta P_2 \end{bmatrix} \Rightarrow \Delta P_m = H_3(s) \Delta P_1 + H_4(s) \Delta P_2 \tag{22}$$

C. *Final forms*

At this stage, the transfer functions relating separately the two external inputs ΔW^* and ΔP_2 to the output ΔW will be established. Initially, ΔP_2=0 is considered. Using (5), (19) and (22) produces

$$\Delta P_1 = K(s) \left[K_p \left(\Delta W^* - \Delta W \right) + \Delta P_f \right] \Rightarrow$$

$$\Delta P_1 = \frac{K_p K(s)}{1 - H(s) H_3(s) K(s)} \Delta W^* - \frac{K_p K(s)}{1 - H(s) H_3(s) K(s)} \Delta W \tag{23}$$

At the same time, (17) and (23) provide

$$\Delta W = H_1(s) \Delta P_1 \Rightarrow$$

$$\Delta W = \frac{K_p K(s) H_1(s)}{1 - H(s) H_3(s) K(s) + K_p K(s) H_1(s)} \Delta W^* \Rightarrow$$

$$\Delta W = G_W(s) \Delta W^* \tag{24}$$

Considering ΔW^*=0, relations (5), (19) and (22) produce

$$\Delta P_1 = K(s) \left[K_p \left(-\Delta W \right) + \Delta P_f \right] \Rightarrow$$

$$\Delta P_1 = \frac{K(s) H(s) H_4(s) \Delta P_2 - K(s) K_p \Delta W}{1 - K(s) H(s) H_3(s)} \tag{25}$$

Finally, using (17) and (25) provides

$$\Delta W = H_1(s) \Delta P_1 + H_2(s) \Delta P_2 \Rightarrow$$

$$\Delta W = \frac{K(s) H(s) H_1(s) H_4(s) + H_2(s) - K(s) H(s) H_2(s) H_3(s)}{1 - H(s) H_3(s) K(s) + K_p K(s) H_1(s)} \Delta P_2 \Rightarrow$$

$$\Delta W = G_P(s) \Delta P_2 \tag{26}$$

The complete expression relating all inputs to the output is

$$\Delta W = G_W(s) \Delta W^* + G_P(s) \Delta P_2 \tag{27}$$

If expanded, both transfer functions $G_W(s)$ and $G_P(s)$ have the same 5th order polynomial as their denominator. Therefore, the investigation in terms of system poles can be performed by examining either of $G_W(s)$ or $G_P(s)$.

IV. RESULTS

Based on the previous mathematical description, a number of study cases are here examined. These will demonstrate the effect of a variation in the VSC control parameters, the transmission link passive components, as well as the nominal operating points, on the poles of $G_W(s)$ in (27). The two investigated VSC-HVDC systems are

- conventional connection of two existing ac grids, referred to as "P2P" connection.
- connection of a wind farm to the main ac grid, referred to as "WF" transmission.

In all of the study cases, the two systems are compared under the same conditions, with their properties defined in Table I, but with the change of selected system values for each different scenario. The steady-state power transfer $P_{2,0}$ and the direct-voltage reference for the direct-voltage controlled station are chosen equal to their nominal values

TABLE I. PROPERTIES OF THE VSC-HVDC SYSTEM

P_N	VSC rated power	1000 MW
$v_{dc,N}$	rated direct voltage	640 kV
$v_{g,N}$	rated alternating voltage at converter side	320 kV
S_N	ac-side rated power	1000 MVA
L_f	phase reactor inductance	50.0 mH
R_f	phase reactor resistance	1.57 Ω
C_{dc}	dc-side capacitor	20 μF
a_d	bandwidth of the closed-loop direct-voltage control	300 rad/s
a_f	bandwidth of the power-feedforward filter	300 rad/s
a_{cc}	bandwidth of the closed-loop current control	3000 rad/s
length	nominal transmission link length	100 km
r	resistance per cable km	0.0146 Ω/km/pole
l	inductance per cable km	0.158 mH/km/pole
c	capacitance per cable km	0.275 mF/km/pole

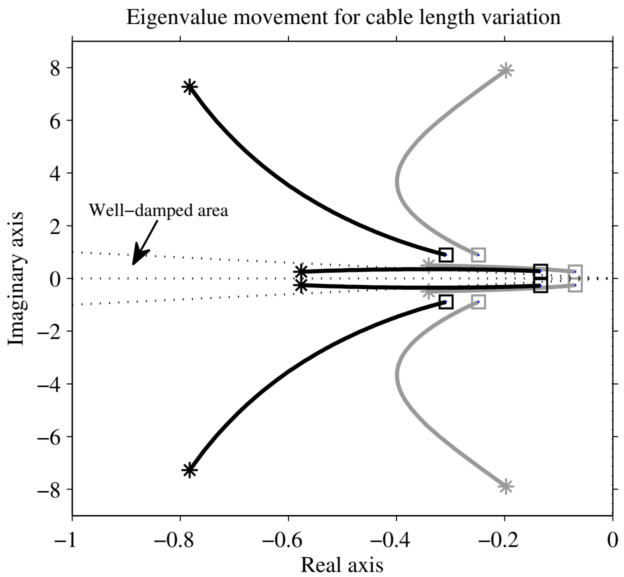

Fig. 3. Pole movement for the P2P (grey) and WF (black) systems for a variation of the dc-transmission link from 50 until 1000 km. Starting point is indicated by an asterisk (*) and ending points by a square (□).

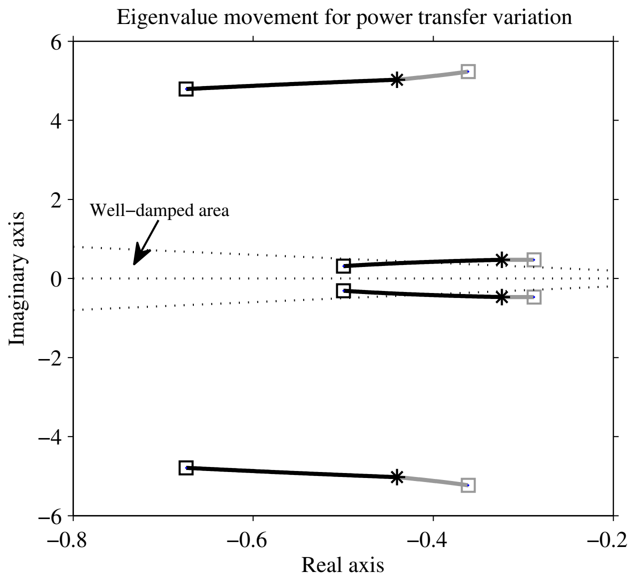

Fig. 4. Pole movement for the P2P (grey) and WF (black) systems for a variation of the transmitted power from 0 until 1000 MW. Starting point is indicated by an asterisk (*) and ending points by a square (□).

from Table I. The other operating points are calculated based on the physical properties of the dc-transmission link. The properties of the latter defined as R_{pole}, L_{pole}, and C_{pole} in Section II, are defined in terms of resistance per cable km r, inductance per cable kilometer l and capacitance per cable kilometer c, respectively. Conventional VSC-HVDC transmission links can feature both overhead- and cable-type of transmission lines. However, the connection of a wind farm (normally offshore) is only performed via cables. Therefore, for consistency in the comparison of the two systems, the properties of r, l and c are here given only for cable type of transmission lines. The parameter values used in $G_W(s)$, as well as the characteristics of the finally extracted poles, are treated in the per unit system.

As observed in all of the case studies, the systems exhibit five poles presented as a very well-damped real pole to the far left of the Left hand of the s-plane (LHP), and two pairs of complex poles (one poorly damped and one relatively well damped) closer to the imaginary axis. The effect of the latter two pole pairs is dominant to the performance of the system and therefore the real pole is not shown in the graphs.

A. Variation of cable length

For the purposes of this scenario, the length of the transmission link is varied from 50-1000km. As observed in Fig. 3, the P2P transmission exhibits poles that, for the same value of cable length, are consistently less damped than those of the WF type of transmission. Specifically, the pair of poorly-damped poles that is associated with the resonance of the dc transmission link (changing its frequency rapidly following the same type of change in the natural frequency of the transmission link) have very poor damping in the P2P case for the smallest values of cable length. Their damping quickly improves for an increase in cable length but is still less than that of the WF transmission. The pair of well-damped poles appears to behave in a similar manner, where larger transmission lengths find the poles closer to the origin. Overall, the dynamic performance of the WF system seems to have better characteristics than its P2P counterpart.

B. Variation of transmitted power

In this study case, the power transmission varies from 0-1000 MW. As expected, due to the similarity of the two systems, their dynamic performance is identical when the power transmission is zero and their poles are found to be placed at the same position, as seen in Fig. 4. However, when the power starts increasing, the two systems behave in exactly opposite way. Both the poorly and well damped poles move closer to the imaginary axis in the P2P case, indicating a degradation of their damping properties, while the real part of the WF system's poles becomes increasingly negative and their damping improves.

This behavior is of great importance when it comes to the poorly-damped pole pair, which are dominant poles in both systems. As a result, an increase in power transfer enhances the overall system dynamics in wind applications but has the opposite effect in the conventional P2P implementations of VSC-HVDC.

C. Simultaneous variation of a_d, a_f and a_{cc}

The bandwidth of the closed-loop current control a_{cc} is typically ten times greater than the a_d. At the same time, the power feedforward filter bandwidth a_f is usually chosen close or equal to a_d [5]. The purpose of this case study is to observe the pole movement of the systems when ad varies, while at the same time respecting the previous guidelines. Consequently, the values of the three previous bandwidths are chosen as provided in Table I and are simultaneously varied by the same multiplying factor, which ranges from 0.5 to 1.5. The results are depicted in Fig. 6.

As it can be observed, once again the WF arrangement has poles that are constantly further from the imaginary axis than their corresponding poles of the P2P transmission system, implying a better damping for the same scaling of the system's bandwidths. An increase of the multiplying

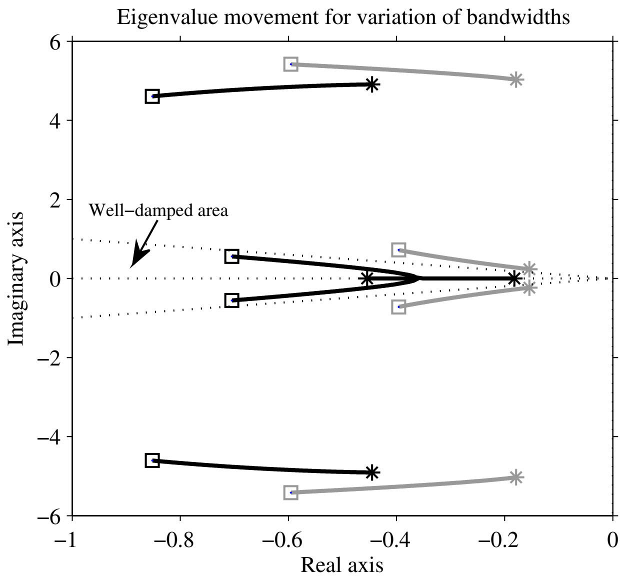

Fig. 6. Pole movement for the P2P (grey) and WF (black) systems for a simultaneous variation of bandwidths a_d, a_f and a_{cc} from 0.5 until 1.5 of their nominal value. Starting point is indicated by an asterisk (*) and ending points by a square (□).

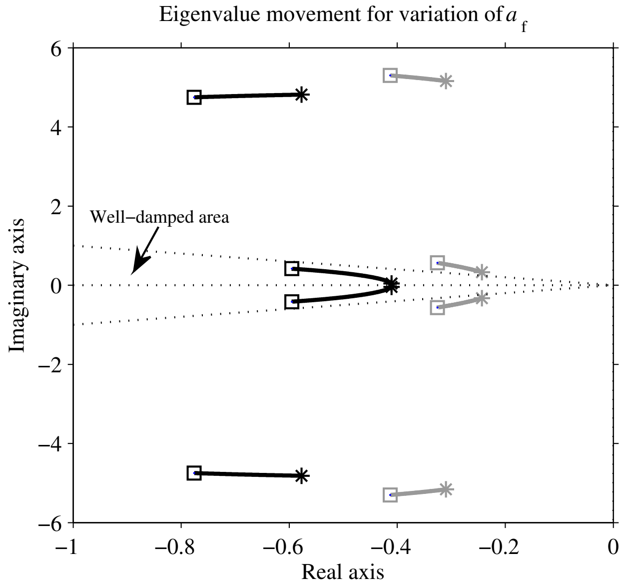

Fig. 5. Pole movement for the P2P (grey) and WF (black) systems for a variation of a_f from 0.5 until 1.5 of its nominal value. Starting point is indicated by an asterisk (*) and ending points by a square (□).

factor causes the poorly-damped poles of both systems to move towards the left of the LHP while virtually maintaining their characteristic frequency, leading to an increase of their damping factor. Conversely, a similar movement towards the left of the LHP is observed for the well-damped pole pair of the systems but with a simultaneous increase of their frequency leading to almost no variation in their damping factor. Nevertheless, the overall stability of both systems improves as the poles increase their distance from the imaginary axis.

D. Variation of a_f with fixed a_d

As mentioned earlier, the bandwidth a_f is usually chosen to be close or equal in value as a_d. The present scenario examines the impact of a varied mismatch between the two bandwidths, while keeping a_d constant. The pole movement results for the two VSC-HVDC systems, regarding a variation of a_f in the range of 0.5-1.5 of its nominal value of 300 rad/s is plotted in Fig. 5. Following as similar trend as the simultaneous change of all bandwidths in the previous study case, an increase of a_f causes all poles of the systems to move towards the left side of the LHP, improving the stability of the systems. Additionally, the poorly-damped poles closely retain their frequency characteristics while the well-damped poles increase their frequency component. A difference compared to Fig. 6 is the fact that for the same variation range of the multiplying factor, the overall movement of the poles is much more limited in the case where only the filter bandwidth is varied. This shows that the simultaneous change of all bandwidths has a much greater impact on the systems than the variation of a single bandwidth.

V. CONCLUSIONS

This paper provides a rigorous description of the dynamic of two-terminal VSC-HVDC transmission systems, examining the case of the conventional power transmission between two existing ac grids and the transmission of power from a wind farm to the mainland grid. Different study cases were considered, exhibiting the persistent existence of poorly-damped poles in both systems. The effect of a wide variation of selected system parameters, was demonstrated via pole-movement investigation of the system's most dominant poles.

Even though similar in mathematical description the two types of VSC-HVDC transmission exhibited great differences in their stability characteristics, owing greatly to the direction of power in the dc-link with regards to the position of the direct-voltage controlled station in the system. The fact that the direct-voltage controlled station is the one acting as an inverter (power-flow direction from dc to ac) for the wind farm case, greatly enhances the stability of the overall system; as a result, for the same type of operating conditions and power transfer, the wind-power transmission scheme was shown to have poles with much better damping, compared to those of the conventional point-to-point power transmission. This of great importance when focusing on the poorly-damped poles, whose properties dominate the overall performance of the systems.

REFERENCES

[1] M. Bahrman, E.V. Larsen, R.J. Piwko and H.S. Patel, "Experience with HVDC - Turbine-Generator Torsional Interaction at Square Butte," IEEE Trans. Power App. Syst., vol. 99, no. 3, pp. 966-975, May 1980.

[2] S.D. Sudhoff, S.F. Glover, P.T. Lamm, D.H. Schmucker and D.E. Delisle, "Admittance space stability analysis of power electronic systems," IEEE Trans. Aerosp. Electron. Syst., vol. 36, no. 3, pp. 965-973, July 2000.

[3] M. Bongiorno and A. Petersson, "Development of a method for evaluation of wind turbines ability to fulfil Swedish grid codes," Vindforsk, Rep. Elforsk Rapport 09:25, Feb. 2009.

[4] L. Harnefors, "Modeling of three-phase dynamic systems using complex transfer functions and transfer matrices," IEEE Trans. Ind. Electron., vol. 54, no. 4, pp. 2239–2248, Aug. 2007.

[5] L. Harnefors,M. Bongiorno and S. Lundberg, "Input-admittance calculation and shaping for controlled voltage-source converters," IEEE Trans. Ind. Electron., vol. 54, no. 6, pp. 3323–3334, Dec. 2007.